Proceedings of CHT-17
ICHMT International Symposium on Advances in Computational Heat Transfer

May 28 – June 1, 2017, Napoli, Italy

CHT-17-279

FORM-DRAG EFFECTS ON UNSTABLE BUOYANT FLOW IN A VERTICAL POROUS LAYER WITH OPEN BOUNDARIES

A. Barletta[*,§], D. A. S. Rees[**]
[*]Dept. of Industrial Engineering, Alma Mater Studiorum Università di Bologna, Italy
[**]Dept. of Mechanical Engineering, University of Bath, UK
[§]Correspondence author. Fax: +39 051 2093296 Email: antonio.barletta@unibo.it

ABSTRACT The onset of convective instability in a vertical porous layer with open boundaries is analysed. The base flow is partly buoyancy-induced and partly caused by an imposed vertical pressure gradient. The linearised perturbation equations expressing the local mass and energy balances, as well as the momentum balance modelled according to Darcy-Forchheimer's law, are solved numerically in terms of normal modes. The neutral stability curves and the critical Darcy-Rayleigh number are obtained versus the form-drag parameter.

INTRODUCTION

The analysis of buoyant flow in a vertical porous layer is of great interest either in engineering or in geophysics. We mention applications to civil engineering such as the design of breathing walls, employed in the dynamical insulation of buildings, or the modelling of groundwater reservoirs. The study of thermoconvective instability in a porous vertical slab with impermeable boundaries kept at different temperatures was first carried out in the pioneering paper by Gill [1969]. This author was able to obtain a fairly simple and elegant proof that the basic parallel buoyant flow in the layer is stable.
The validity of Gill's proof strongly relies on the boundary conditions of impermeable isothermal walls. This finding has been reported by Barletta [2015]. In fact, when the layer boundaries are permeable with a pressure equal to the fluid hydrostatic pressure, the parallel buoyant flow may become unstable [Barletta, 2015].
Both Gill's proof and its later development [Barletta, 2015] depend on the assumption that momentum transport is modelled through Darcy's law. In fact, Darcy's law is an appropriate model of seepage flow in a porous medium whenever the permeability-based Reynolds number,

$$Re_K = \frac{|\mathbf{u}^*| \sqrt{K}}{\nu}, \tag{1}$$

is small enough [Nield and Bejan, 2013]. Here, $\mathbf{u}^*$ is the seepage velocity, K is the permeability, and ν is the kinematic viscosity of the fluid. Breakdown of Darcy's law initiates when Re_K is $O(1)$. For larger values of Re_K, Darcy's law relative to buoyant flows needs to be corrected through a quadratic drag term,

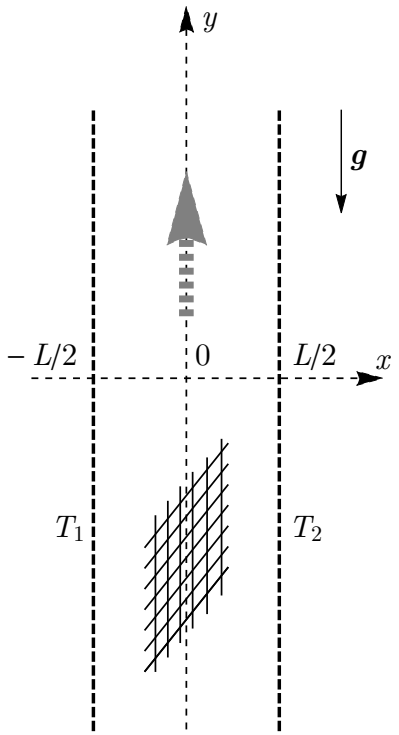

Figure 1. Two-dimensional sketch of the vertical porous layer

so that it can be written as [Nield and Bejan, 2013]

$$\frac{\mu}{K}\left(1 + c_F\, Re_K\right)\mathbf{u}^* = -\boldsymbol{\nabla} P^* - \rho\gamma\mathbf{g}\left(T^* - T_0\right), \tag{2}$$

where μ is dynamic viscosity; c_F is the form-drag coefficient; P^* is the local difference between the pressure and the hydrostatic pressure, hereafter called dynamic pressure; ρ is the reference density for the buoyancy force; γ is the thermal expansion coefficient of the fluid; $\mathbf{g}$ is the gravitational acceleration; T^* is the temperature and T_0 is the reference temperature. Darcy's law with the quadratic drag correction is also well-known as Darcy-Forchheimer's law. Several studies about the influence of quadratic drag correction on the onset of thermal instability in saturated porous media are available in the literature. Among the many, we mention Rees [1997]; Rees et al. [2006]; Delache et al. [2007]; Barletta et al. [2009]; and Barletta and Rees [2015].

The aim of this paper is to extend the results obtained by Barletta [2015] to a regime where the quadratic drag correction to Darcy's law is important. A vertical porous layer with open boundaries maintained at different temperatures will be considered. Darcy-Forchheimer's law, within the framework of the Oberbeck-Boussinesq approximation, will be employed to develop the stability analysis. A linear study will be carried out, aimed to obtain the neutral stability curves, and the critical values for the onset of convective instability. The linear stability analysis entails the numerical solution of an eigenvalue problem. Here, this solution will be tackled by a combined use of an initial value ODE solver and the shooting method.

MATHEMATICAL MODEL

We consider the vertical plane porous layer sketched in Fig. 1. The fluid-saturated porous medium is modelled as homogeneous and isotropic. The $x-$axis and $z-$axis are horizontal, while the $y-$axis is

vertical, so that the gravitational acceleration is given by $\mathbf{g} = -g\,\mathbf{e}_y$. Here, g is the modulus of $\mathbf{g}$ and $\mathbf{e}_y$ is the unit vector along the $y-$axis. We assume that the quadratic drag effect cannot be neglected, so that Darcy–Forchheimer's law holds. We further assume that the Oberbeck–Boussinesq approximation can be applied and that local thermal equilibrium holds.
In agreement with these assumptions and with Eqs. (1) and (2), the local mass, momentum and energy balance equations can be expressed in a dimensionless form as,

$$\boldsymbol{\nabla}\cdot\mathbf{u} = 0, \tag{3a}$$

$$(1+\xi|\mathbf{u}|)\,\mathbf{u} = -\boldsymbol{\nabla}P + T\mathbf{e}_y, \tag{3b}$$

$$\frac{\partial T}{\partial t} + \mathbf{u}\cdot\boldsymbol{\nabla}T = \nabla^2 T, \tag{3c}$$

with the boundary conditions

$$x = \pm 1/2: \qquad P = 0, \qquad T = \pm\frac{R}{2}. \tag{4}$$

In Eqs. (3) and (4), the dimensionless coordinates, time, velocity, dynamic pressure and temperature have been denoted as: $\mathbf{x} = (x,y,z)$, t, $\mathbf{u} = (u,v,w)$, P and T, respectively. The boundary conditions at $x = \pm 1/2$ express the continuity of pressure between the fluid saturating the porous layer and the external reservoirs, where the pressure distribution coincides with the hydrostatic pressure.
The dimensionless variables are defined as

$$\begin{aligned} &(x^*,y^*,z^*)\,\frac{1}{L} = (x,y,z), \qquad t^*\,\frac{\alpha}{\sigma L^2} = t, \qquad (u^*,v^*,w^*)\,\frac{L}{\alpha} = (u,v,w),\\ &P^*\,\frac{K}{\mu\alpha} = P, \qquad (T^*-T_0)\,\frac{g\gamma KL}{\nu\alpha} = T. \end{aligned} \tag{5}$$

Here, the asterisks denote the dimensional coordinates, time, velocity, pressure and temperature; α is the average thermal diffusivity; K is the permeability; σ is the heat capacity ratio, *viz.* the ratio between the average volumetric heat capacity of the fluid–saturated porous medium and the volumetric heat capacity of the fluid. Moreover, the reference temperature introduced for the definition of buoyancy force is the arithmetic mean of the wall temperatures, $T_0 = (T_1+T_2)/2$.
The dimensionless parameters R and ξ are the Darcy–Rayleigh number and the form–drag parameter, respectively,

$$R = \frac{g\gamma(T_2-T_1)KL}{\nu\alpha}, \qquad \xi = \frac{c_f\alpha\sqrt{K}}{\nu L}. \tag{6}$$

It is not restrictive to carry out our analysis with $R > 0$, meaning that $T_2 > T_1$.

THE BASIC BUOYANT FLOW

A stationary solution of Eqs. (3) and (4) may be found and it is given by

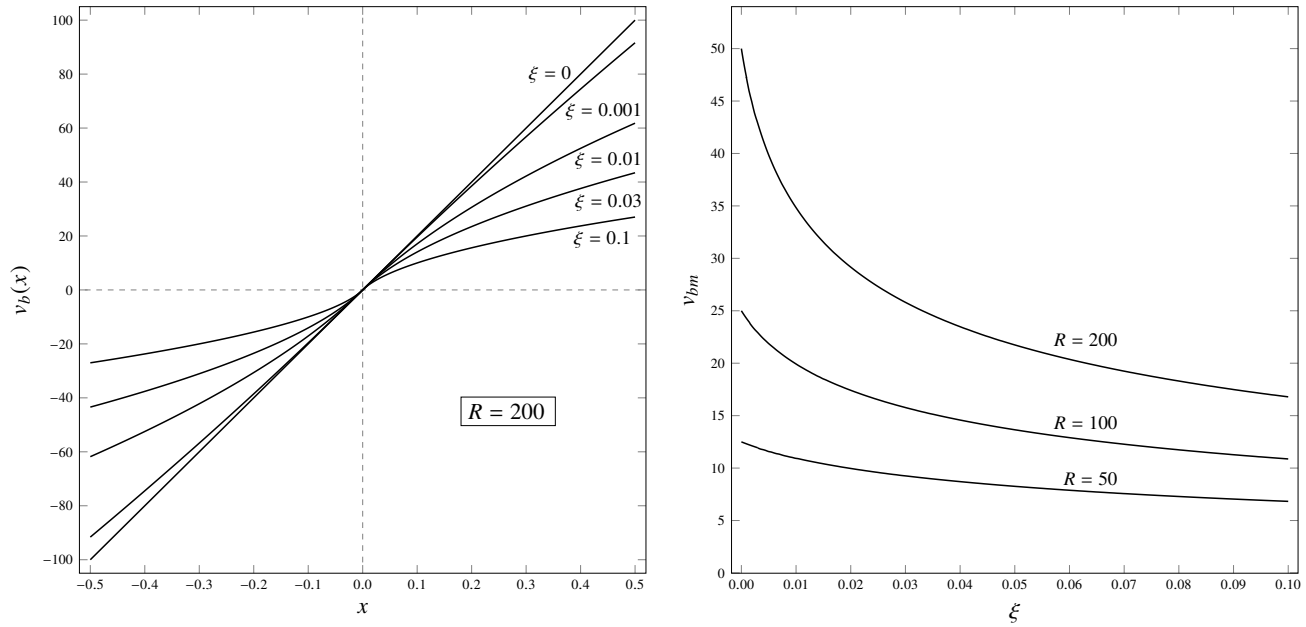

Figure 2. Basic flow: velocity profiles, $v_b(x)$, evaluated for $R = 200$ and different values of ξ; average velocity, v_{bm}, versus ξ evaluated for different values of R

$$u_b = 0, \quad v_b = \frac{2Rx}{1 + \sqrt{4R\xi\,|x| + 1}}, \quad w_b = 0, \quad T_b = Rx, \quad P_b = 0, \tag{7}$$

where the subscript b denotes the basic state. Equation (7) describes a parallel vertical flow where the velocity is directed upward for $x \in [0, 1/2]$ and downward for $x \in [-1/2, 0]$. The velocity profile $v_b(x)$ is given by an odd function of x. The average velocity in the hotter half-channel, $x \in [0, 1/2]$, is given by

$$v_{bm} = \frac{(1 + 2R\xi)^{3/2} - 3R\xi - 1}{6R\xi^2} = \frac{R}{3}\left[\frac{1 + 2\sqrt{1 + 2R\xi}}{(1 + \sqrt{1 + 2R\xi})^2}\right]. \tag{8}$$

In the limiting case $\xi \to 0$, *viz.* the case of Darcy's flow, Eq. (7) yields $v_b = T_b = Rx$, while Eq. (8) yields $v_{bm} = R/4$. Thus, the regime of Darcy's flow implies the linear velocity profile studied by both Gill [1969] and Barletta [2015].

The effect of the form-drag parameter ξ is illustrated in Fig. 2. Plots of the velocity profile $v_b(x)$ are displayed in this figure for $R = 200$ and increasing values of ξ. One may note the progressive departure from the linear velocity profile as ξ increases above zero. An increasing ξ means a decreasing average flow velocity in the hotter half-channel, v_{bm}. This feature holds for different values of R as shown by the right-hand frame of Fig. 2.

STABILITY ANALYSIS

In order to test the stability of the basic state, given by Eqs. (7), we express the perturbed velocity and temperature as

$$\mathbf{u} = \mathbf{u}_b + \varepsilon\,\tilde{\mathbf{u}}, \qquad T = T_b + \varepsilon\,\tilde{T}, \qquad P = P_b + \varepsilon\,\tilde{P}, \tag{9}$$

where ε is the perturbation parameter, while $\tilde{\mathbf{u}} = (\tilde{u}, \tilde{v}, \tilde{w})$ and $\tilde{T}$ are the perturbation fields. Consistently with a linear stability analysis, we will assume that $|\varepsilon| \ll 1$. Therefore, nonlinear terms in the perturbation fields will be considered as negligible in Eqs. (3) and (4) and we may write the governing equations and boundary conditions as

$$\frac{\partial \tilde{u}}{\partial x} + \frac{\partial \tilde{v}}{\partial y} + \frac{\partial \tilde{w}}{\partial z} = 0, \tag{10a}$$

$$(1 + \xi|v_b|)\,\tilde{u} = -\frac{\partial \tilde{P}}{\partial x}, \tag{10b}$$

$$(1 + 2\xi|v_b|)\,\tilde{v} = -\frac{\partial \tilde{P}}{\partial y} + \tilde{T}, \tag{10c}$$

$$(1 + \xi|v_b|)\,\tilde{w} = -\frac{\partial \tilde{P}}{\partial z}, \tag{10d}$$

$$\frac{\partial \tilde{T}}{\partial t} + R\tilde{u} + v_b \frac{\partial \tilde{T}}{\partial y} = \frac{\partial^2 \tilde{T}}{\partial x^2} + \frac{\partial^2 \tilde{T}}{\partial y^2} + \frac{\partial^2 \tilde{T}}{\partial z^2}, \tag{10e}$$

$$x = \pm 1/2: \qquad \tilde{P} = 0, \qquad \tilde{T} = 0. \tag{10f}$$

Equations (10) may be rearranged so that the disturbance governing equations are formulated in terms of the unknowns $(\tilde{T}, \tilde{P})$,

$$\frac{\partial}{\partial x}\left[(1 + \xi|v_b|)^{-1}\frac{\partial \tilde{P}}{\partial x}\right] + (1 + 2\xi|v_b|)^{-1}\frac{\partial^2 \tilde{P}}{\partial y^2} + (1 + \xi|v_b|)^{-1}\frac{\partial^2 \tilde{P}}{\partial z^2} - (1 + 2\xi|v_b|)^{-1}\frac{\partial \tilde{T}}{\partial y} = 0, \tag{11a}$$

$$\frac{\partial \tilde{T}}{\partial t} - R\,(1 + \xi|v_b|)^{-1}\frac{\partial \tilde{P}}{\partial x} + v_b \frac{\partial \tilde{T}}{\partial y} = \frac{\partial^2 \tilde{T}}{\partial x^2} + \frac{\partial^2 \tilde{T}}{\partial y^2} + \frac{\partial^2 \tilde{T}}{\partial z^2}, \tag{11b}$$

$$x = \pm 1/2: \qquad \tilde{P} = 0, \qquad \tilde{T} = 0. \tag{11c}$$

We now express the perturbation fields $(\tilde{T}, \tilde{P})$ in terms of normal modes

$$\tilde{T} = h(x)\, e^{i(\alpha y + \beta z)}\, e^{\eta t}, \quad \tilde{P} = f(x)\, e^{i(\alpha y + \beta z)}\, e^{\eta t}, \tag{12}$$

where $\mathbf{k} = (0, \alpha, \beta)$ is the wave vector, $k = (\alpha^2 + \beta^2)^{1/2}$ is the wave number and η is a a complex quantity, $\eta = q - i\omega$, such that q is the growth-rate parameter and ω is the angular frequency. Stability occurs when $q < 0$, while instability occurs when $q > 0$. The onset of instability is defined by the parametric condition $q = 0$, *viz.* the neutral stability condition.
Substitution of Eq. (12) into Eqs. (11) yields the stability eigenvalue problem,

$$D\left[(1 + \xi|v_b|)^{-1} Df\right] - \alpha^2 (1 + 2\xi|v_b|)^{-1} f - \beta^2 (1 + \xi|v_b|)^{-1} f - i\alpha\,(1 + 2\xi|v_b|)^{-1} h = 0, \tag{13a}$$

$$D^2 h - \left(k^2 + \eta + i\alpha v_b\right) h + R\,(1 + \xi|v_b|)^{-1} Df = 0, \tag{13b}$$

$$x = \pm 1/2: \qquad f = 0, \qquad h = 0, \tag{13c}$$

where $D = d/dx$. We note that $\alpha = 0$ defines the special case of longitudinal rolls, and $\beta = 0$ that of transverse rolls. The range of oblique rolls is spanned by a continuous change from longitudinal to transverse rolls. This may be accomplished by writing,

$$\alpha = \sqrt{s}\, k, \quad \beta = \sqrt{1-s}\, k, \quad s \in [0,1]. \tag{14}$$

Thus, Eqs. (13) can be rewritten as

$$\begin{aligned} D\left[(1+\xi|v_b|)^{-1} Df\right] - sk^2 (1+2\xi|v_b|)^{-1} f - (1-s)k^2 (1+\xi|v_b|)^{-1} f \\ - i\sqrt{s}\, k (1+2\xi|v_b|)^{-1} h = 0, \end{aligned} \tag{15a}$$

$$D^2 h - \left(k^2 + \eta + i\sqrt{s}\, k v_b\right) h + R (1+\xi|v_b|)^{-1} Df = 0, \tag{15b}$$

$$x = \pm 1/2 : \qquad f = 0, \qquad h = 0. \tag{15c}$$

Longitudinal rolls In the special case of longitudinal rolls ($s = 0$), Eqs. (15) undergo a dramatic simplification,

$$D\left[(1+\xi|v_b|)^{-1} Df\right] - k^2 (1+\xi|v_b|)^{-1} f = 0, \tag{16a}$$

$$D^2 h - \left(k^2 + \eta\right) h + R (1+\xi|v_b|)^{-1} Df = 0, \tag{16b}$$

$$x = \pm 1/2 : \qquad f = 0, \qquad h = 0. \tag{16c}$$

If one multiplies Eq. (16a) by the complex conjugate of f, namely $\bar{f}$, one integrates by parts over the range $x \in [-1/2, 1/2]$, and one employs the boundary conditions (16c), one obtains

$$\int_{-1/2}^{1/2} (1+\xi|v_b|)^{-1} |Df|^2\, dx + k^2 \int_{-1/2}^{1/2} (1+\xi|v_b|)^{-1} |f|^2\, dx = 0. \tag{17}$$

This equation can be satisfied for any $k > 0$ if and only if $f = 0$. Thus, Eqs. (16) are further simplified to

$$D^2 h - \left(k^2 + \eta\right) h = 0, \tag{18a}$$

$$x = \pm 1/2 : \qquad h = 0. \tag{18b}$$

The solution of Eqs. (18) can be expressed as

$$h = A \sinh\left[\sqrt{k^2+\eta}\left(x + \frac{1}{2}\right)\right], \tag{19}$$

Table 1
Oblique rolls with $s = 0.5$, $k = 1$, $\xi = 0.01$: comparison between the neutral stability values of $(R, \omega, \chi_1, \chi_2)$ obtained by a fixed step-size Runge-Kutta solver having gradually decreasing step-size, $\delta x = 10^{-N}$, with an adaptive step-size Runge-Kutta solver

N	R	ω	χ_1	χ_2
2.0	574.1487250	0.04503138296	0.02467819404	−0.02698728304
2.2	574.1418746	0.01706300442	0.02467057185	−0.02698226496
2.4	574.1168419	0.01122028490	0.02466927057	−0.02698158035
2.6	574.1294156	−0.00742607738	0.02466398575	−0.02697797823
2.8	574.1257225	−0.00099288777	0.02466580072	−0.02697921064
3.0	574.1273572	0.00453439813	0.02466730147	−0.02698019606
3.2	574.1269008	−0.00099909809	0.02466578455	−0.02697919140
3.4	574.1271954	0.00113458682	0.02466636797	−0.02697957693
3.6	574.1270999	0.00026781778	0.02466613067	−0.02697941994
3.8	574.1271471	−0.00028493251	0.02466597801	−0.02697931817
4.0	574.1271384	0.00045379328	0.02466618136	−0.02697945334
adaptive	574.1271085	−0.00017646296	0.02466600834	−0.02697933857

where A is an arbitrary nonzero constant and

$$k^2 + \eta = -n^2\pi^2, \qquad n = 1, 2, 3, \ldots . \tag{20}$$

Since $\eta = q - i\omega$, one may infer that $\omega = 0$ and that $q < 0$. Therefore, the conclusion is that longitudinal rolls are always stable.

The Asymptotic Regime of Darcy's Flow When $\xi \to 0$, the effects of quadratic drag vanish and the local momentum balance equation is given by Darcy's law. In this regime, the basic velocity profile is $v_b = Rx$. Then, Eqs. (15) are simplified to

$$D^2 f - k^2 f - i\sqrt{s}\, k h = 0, \tag{21a}$$

$$D^2 h - \left(k^2 + \eta + i\sqrt{s}\, kRx\right) h + RDf = 0, \tag{21b}$$

$$x = \pm 1/2: \qquad f = 0, \qquad h = 0. \tag{21c}$$

The eigenvalue problem (21) coincides with that studied by Barletta [2015].

Numerical Method The stability eigenvalue problem (15) can be solved for a fixed growth rate $q = 0$. Such a solution provides the neutral stability data that can be reported as values of R versus the wave number k, represented graphically in the (k, R) plane. The computation must be carried out for prescribed values of the pair (s, ξ). There are several strategies to tackle the numerical solution of stability eigenvalue problems; most of them are surveyed in chapter 19 of Straughan [2004]. The solution method adopted here is the shooting method. This method is based on a numerical integration of the initial value problem based on Eqs. (15a), (15b), and on a suitable set of initial conditions prescribed at $x = -1/2$,

$$f(-1/2) = 0, \qquad f'(-1/2) = \chi_1 + i\chi_2, \qquad h(-1/2) = 0, \qquad h'(-1/2) = 1. \tag{22}$$

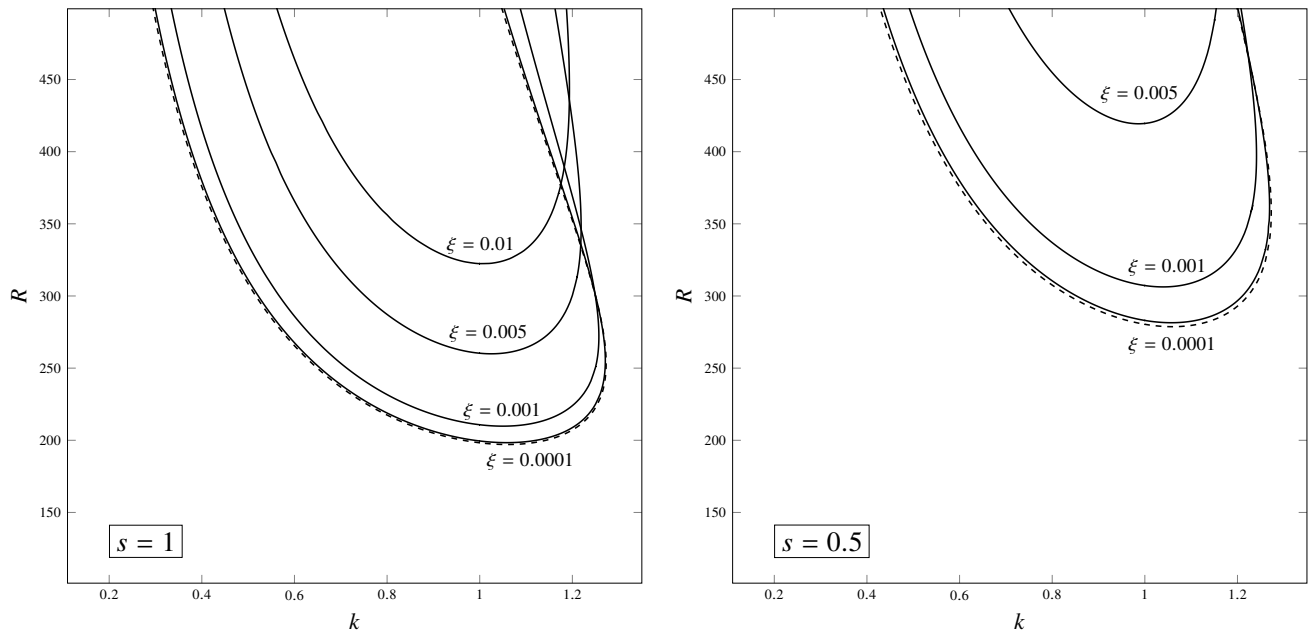

Figure 3. Neutral stability curves for different values of ξ with either $s = 1$ (transverse rolls) or $s = 0.5$ (oblique rolls). The dashed lines identify the limiting case of Darcy's flow, $\xi \to 0$

Equation (22) is compatible with Eq. (15c), but the last condition breaks the scale invariance of a differential problem that, otherwise, is homogeneous. The parameters (χ_1, χ_2) are a-priori undetermined. For input data (k, s, ξ) and $q = 0$, the unknowns $(R, \omega, \chi_1, \chi_2)$ are determined by the end conditions prescribed at $x = 1/2$, namely

$$f(1/2) = 0, \qquad h(1/2) = 0. \tag{23}$$

The shooting method consists in solving numerically Eq. (23) to yield the values of $(R, \omega, \chi_1, \chi_2)$. The software environment *Mathematica* (© Wolfram Research) provides adequate tools to develop the shooting method: function `NDSolve` for the numerical solution of the differential initial value problem, and function `FindRoot` for finding the roots of Eq. (23). The option `Method` of function `NDSolve` is set to 4^{th} order Runge-Kutta method. Within *Mathematica*, the default engine of Runge-Kutta method is an adaptive strategy with variable step-size δx over the computational range $x \in [-1/2, 1/2]$, but the numerical accuracy of the output can be monitored by comparing it with that obtained by setting a fixed step-size with a given δx. This test is exploited in Table 1 where the output data $(R, \omega, \chi_1, \chi_2)$ are reported for fixed and gradually decreasing δx, and compared with the adaptive strategy, for variable δx. The input data in Table 1 are $(k, s, \xi) = (1, 0.5, 0.01)$. We note that the discrepancy between the data relative to a fixed step-size $\delta x = 10^{-4}$ and those for the adaptive strategy is less than 6×10^{-6} % for R, less than 8×10^{-4} % for χ_1, and less than 5×10^{-4} % for χ_2. The values of ω conveyed in Table 1 are a different matter. The trend of ω as δx decreases, and the comparison with the value of ω obtained when the adaptive step-size strategy is adopted show that ω is effectively zero. The same behaviour is recorded for all the neutral stability data exhibited in this paper, meaning that the onset of instability is achieved through non-travelling modes. All forthcoming numerical results are obtained by employing the adaptive step-size strategy.

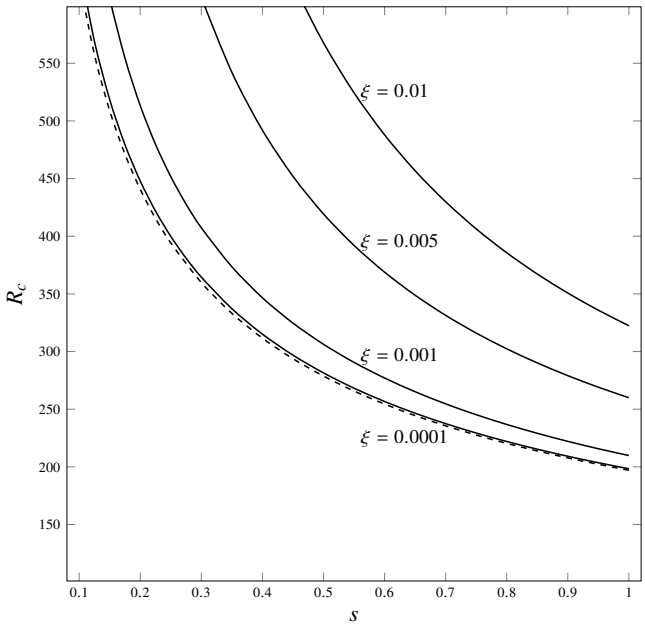

Figure 4. Critical value of R versus s for different values of ξ. The dashed line identifies the limiting case of Darcy's flow, $\xi \to 0$

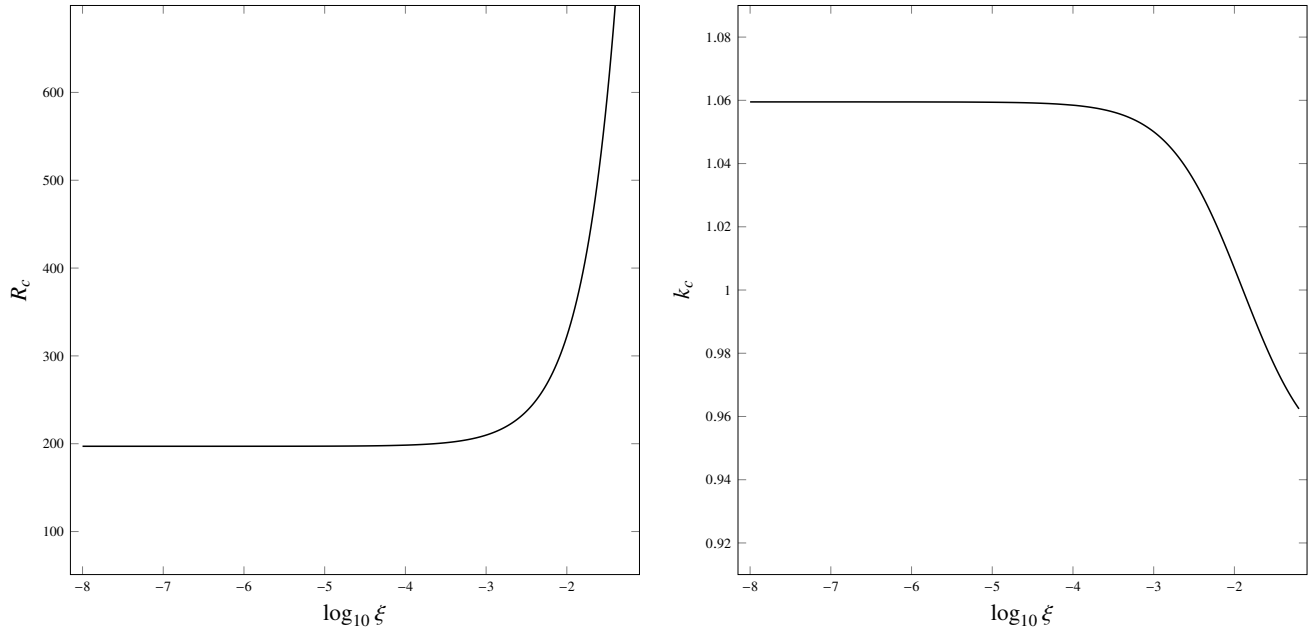

Figure 5. Transverse modes ($s = 1$): critical values of R and k versus ξ

DISCUSSION OF THE RESULTS

The graphical behaviour of R versus k is the neutral stability curve defining the threshold of convective instability. In the plane (k, R), the region of instability is above the neutral stability curve, so that the minimum of R along the curve connotes the critical wave number k_c for the onset of instability, and the associated critical Rayleigh number R_c. Different neutral stability curves are obtained for different values of s and ξ.

Table 2
Transverse modes ($s = 1$): values of R_c and k_c versus ξ

ξ	R_c	k_c
0	197.081	1.05950
10^{-6}	197.094	1.05949
10^{-5}	197.209	1.05939
0.0001	198.359	1.05846
0.001	209.796	1.05007
0.005	259.937	1.02492
0.01	322.368	1.00687
0.02	448.012	0.98755

Figure 3 shows the neutral stability curves for either transverse rolls, $s = 0$, or oblique rolls having $s = 0.5$. It is easily inferred from Eq. (14) that $s = 0.5$ entails oblique modes whose wave vector $\mathbf{k}$ is inclined an angle $\pi/4$ to the vertical in the zy plane. Several values of ξ are taken in Fig. 3, ranging from 0.0001 to 0.01. The dashed lines present a comparison with the limiting case of Darcy's flow ($\xi \to 0$) analysed in Barletta [2015]. The two main inferences stemming from Fig. 3 are that the quadratic drag correction to Darcy's law has a stabilising effect, and that oblique rolls are more stable than transverse rolls for any given ξ. We mention that the curve with $\xi = 0.01$ lies above the plotted range when $s = 0.5$. We also mention that, even with a value of ξ as small as 0.001, the departure from Darcy's law is quite evident. The general shape of the neutral stability curves for nonzero ξ mimics that for $\xi \to 0$ [Barletta, 2015]. In particular, for given (s, ξ), there exists a point of maximum wave number above which no transition to instability is detected.
The dependence of the critical value of R on parameter s is illustrated in Fig. 4. This figure supports quite clearly the conclusion that oblique rolls ($s < 1$) are always less unstable than transverse rolls. The range examined is restricted to $s \in [0.1, 1]$ having in mind that longitudinal rolls ($s = 0$) are always stable ($R_c \to +\infty$). Figure 5 shows the change of R_c and that of k_c versus ξ with reference to transverse rolls. The asymptotic regime of Darcy's law ($\xi \to 0$) is clearly displayed. It can be approximately identified with the range $\xi < 10^{-4}$. For larger values of ξ, R_c increases and k_c decreases, which is consistent with the plots shown in Fig. 3. Values of R_c and k_c for transverse modes and diverse ξ ranging from 0 to 1 are reported in Table 2. In particular, the values of R_c and k_c for $\xi = 0$ are identical, within 6 significant figures, to those obtained by Barletta [2015].

CONCLUSIONS

The buoyancy-induced parallel flow in a vertical plane porous layer has been analysed. The momentum transfer model includes the quadratic drag contribution, parametrised by the dimensionless number ξ. The effect of increasing ξ from zero results in a modification of the fully-developed basic velocity profile relative to the Darcy's flow linear profile. The boundaries of the porous layer are considered as isothermal, with unequal temperatures, and open to external fluid reservoirs.
The linear stability of the base parallel flow has been investigated through a normal modes analysis. The stability eigenvalue problem has been solved numerically by employing the shooting method. The study has been carried out by a three-dimensional formulation including oblique modes ranging from longitudinal to transverse. The longitudinal modes have been proved to be always stable, while oblique modes are always more stable than transverse modes. Transverse modes yield periodic two-dimensional convection cells lying in the plane of the base flow.
The effect of the quadratic drag on the onset of convective instability is stabilising, meaning that the

critical wave number for the onset of instability continuously increases with parameter ξ. This effect yields a sensible change of the threshold conditions for instability when ξ is 10^{-4} or larger.

REFERENCES

Barletta, A., [2015]. A proof that convection in a porous vertical slab may be unstable. J. Fluid Mech., Vol. 770, pp. 273–288.

Barletta, A., Celli, M., Rees, D. A. S., [2009]. Darcy-Forchheimer flow with viscous dissipation in a horizontal porous layer: onset of convective instabilities. ASME J. Heat Transf., Vol. 131, no. 072602.

Barletta, A., Rees, D. A. S., [2015]. Form-drag effects in the convective instability of parallel flow in a horizontal porous layer with uniform wall heating. In: ICHMT Digital Library Online
(doi: 10.1615/ICHMT.2015.IntSympAdvComputHeatTransf.1480). Begell House Inc.

Delache, A., Ouarzazi, M. N., Combarnous, M., [2007]. Spatio-temporal stability analysis of mixed convection flows in porous media heated from below: Comparison with experiments. Int. J. Heat Mass Tran., Vol. 50, pp. 1485–1499.

Gill, A. E., [1969]. A proof that convection in a porous vertical slab is stable. J. Fluid Mech., Vol. 35, pp. 545–547.

Nield, D. A., Bejan, A., [2013]. Convection in Porous Media, 4th Edition. Springer-Verlag, New York.

Rees, D. A. S., [1997]. The effect of inertia on the onset of mixed convection in a porous layer heated from below. Int. Commun. Heat Mass, Vol. 24, pp. 277–283.

Rees, D. A. S., Postelnicu, A., Storesletten, L., [2006]. The onset of Darcy-Forchheimer convection in inclined porous layers heated from below. Transport Porous Med., Vol. 64, pp. 15–23.

Straughan, B., [2004]. The Energy Method, Stability, and Nonlinear Convection, 2nd Edition. Springer, New York, NY.